1-1-2010

Automatic human motion classification from Doppler spectrograms

Fok Hing Chi Tivive
University of Wollongong, tivive@uow.edu.au

Abdesselam Bouzerdoum
University of Wollongong, bouzer@uow.edu.au

Moeness G. Amin
Villanova University, mamin@uow.edu.au

Automatic human motion classification from Doppler spectrograms

Automatic Human Motion Classification from Doppler Spectrograms

Fok Hing Chi Tivive, Abdesselam Bouzerdoum
School of Electrical, Computer and Telecommunications Engineering
University of Wollongong, Wollongong, NSW 2522, Australia
Email: {tivive, a.bouzerdoum}@uow.edu.au

Moeness G. Amin
Center for Advanced Communications
Villanova University, Villanova, PA 19085, USA
Email: moeness.amin@villanova.edu

***Abstract*—A technique, recently introduced for visual pattern classification, is successfully applied for classification of human gait based on radar Doppler signatures depicted in the time-frequency domain. It is shown that the proposed classification technique implements steps that, in essence, act on revealing the distinctive Doppler features of the human walking and, as such, allows effective discrimination of various types of human motions characterized by the nature of arm swings. We specifically consider three types of arm motions, namely, free swings, one-arm confined swings, and no-arm swings. The last two arm motions can be indicative of a human carrying objects or a person in stressed situations. The paper explains the different processing stages of motion classification architecture and demonstrates their contributions to the final decision.**

I. Introduction

Time-frequency signal representations convert a one-dimensional non-stationary temporal signal into a two-dimensional joint-variable distribution [1]–[5]. Signals characterized with multiple components with different frequency laws leave distinct features when examined in the time-frequency domain [6]. The time-frequency signal representation, which depicts the signal power distribution over time and frequency, can be cast as a typical image in which the two spatial axes are replaced by time and frequency variables. This similarity invites the application of image-based classification techniques to non-stationary signal analyses.

In this paper, we apply an image-based classification technique to distinguish between various types of human gait. In this respect, we consider radar data returns of human walking motion and represent the corresponding signal in the time-frequency domain using spectrograms. In particular three types of motions are of interest: 1) Free arm-motion (FAM) characterized by swinging of both arms, 2) Partial arm-motion (PAM) which corresponds to a motion of only one arm, and 3) No arm-motion (NAM) which corresponds to no motion of both arms. The NAM is referred to as a stroller or sauntere [7]. The last two classes are commonly associated with a person walking with his/her hand(s) in the trouser pockets or a person carrying light small or large heavy objects, respectively. All three categories are considered important for police and law enforcement, especially when humans are inside buildings and in enclosed structures, or they are monitored while moving in city canyons and street corners, or being tracked behind opaque material such as walls in surveillance operations.

The radar micro-Doppler has effectively been used for human gait understanding and classification [8], [9]. Existing works in human motion classification can be categorized into two different classes. The first class is parametric, in which explicit parameters are extracted from the respective time-frequency distributions and used as features for classification [10]. Some important features could be the periods characterizing the repetitive arm and leg motions, the Doppler frequency of the torso which is indicative to whether it is a walking or running motion, the RCS values, the relative times of positive and negative Doppler describing the forward and backward swings, and others. The second class is non-parametric in which portions or segments of the time-frequency distributions, or their subspace representations, are employed as features, followed by a classifier [11], [12].

Our contribution to the above gait classification problem belongs to the second class, i.e., it is nonparametric in nature. It stems from the similarity in dealing with a two dimensional data whether it belongs to an optical image or a time-frequency representation. Image processing through directional and adaptive two-dimensional filters are applied to the time-Doppler frequency distribution of the radar returns to highlight and extract distinctive features corresponding to the above three motion types. Recently, these filters have been successfully used as part of a new hierarchical architecture for visual pattern classification [13]. We show that those filters, when acting on the human gait Doppler signatures strive to capture the underlying and salient features describing the nature of the arm motions and, as such, yield very attractive classification rates.

This paper is organized as follows. Section II describes the application of Short-Time Fourier Transform (STFT) technique to capture the micro-Doppler effects of the three types of arm motions: FAM, PAM and NAM induced on the radar returns. A description of the proposed classification method is given in Section III. Section IV presents experimental results showing that the proposed image processing technique can be successfully applied to time-frequency signal representations. Finally, concluding remarks are given in Section V.

II. Human Motion Signatures in Time-Frequency

The proposed classification technique is applied to real data collected in the Radar Imaging Lab, Center for Advanced

978-1-4244-6459-3/10/$26.00 ©2010 IEEE

Communications, Villanova University, USA. The radar is a continuous wave (CW) operating at 2.4 GHz and with direct line of sight to the target. The data for five persons (labelled as A, B, C, D and E) were collected and sampled at 1 KHz with a transmit power level of 5 dBm. The motion of each subject was recorded for 20 seconds, with the person moving forwards (towards the radar) and backwards.

The spectrogram, which shows how the spectral density of a signal varies with time, is used to analyze the time-varying micro-Doppler signatures of human motions. It is obtained by computing the Short-Time Fourier Transform (STFT) with a hamming window. Figures 1(a)-(c) illustrate the Doppler spectrograms of the three arm motions: PAM, FAM and NAM. The spine of each plot represents the torso motion, i.e., the speed of the subject, whereas the positive and negative Dopplers correspond to the subject moving toward or away from the radar, respectively. The periodic peaks in the plots denote the arms, legs and foot motions. For instance, in Fig. 1(a), fast arm motions are shown as large peaks, whereas the foot and leg motions appear as smaller peaks. Note that during a gait cycle the arm motion produces a positive and a negative Doppler, and the leg motion generates positive Doppler for a subject moving towards the radar and a negative Doppler for a subject moving backwards facing the radar [12]. The reason is that for the approaching subject the legs are always moving forwards, or at most stationary, during limb support phase. Figure 1(b) depicts the composite Doppler for the legs, the arms and the feet when the subject is swinging both arms while walking. These spectrograms show clearly that there is a difference between human gait signatures. Hence, the objective of this paper is to apply an image-based classification technique to highlight the intrinsic characteristics of the gait signatures and subsequently extract salient features for classifying different human activities.

III. Hierarchical Image Classification Architecture

In [10] the classification of human activity was achieved by first extracting a set of features from the entire Doppler spectrogram, then feeding them to a support vector machine (SVM) classifier; naturally, the performance of the classifier depends on the type and number of features selected as inputs to the classifier. In this paper, classification of human walking motion is achieved using a hierarchical image classification architecture (HICA) that operates directly on short time-frequency windows. The raw spectrogram windows are processed and classified automatically into one of three arm motion types: FAM, PAM and NAM. The HICA, shown in Fig. 2, consists of three processing stages. The first stage extracts motion energy and directional contrast in the time-frequency plane. The role of the second stage is to learn the intrinsic features characterizing the different classes of arm motion during human walk. The last stage is a classifier that uses as input the learned features of the second stage. The first two stages employ nonlinear processing inspired by the biophysical mechanism of *shunting inhibition*, which plays an important role in many visual functions [14], [15]; it has been adopted in machine learning [16]–[18] and image processing [19], [20]. The following subsections describe the three processing stages in more detail.

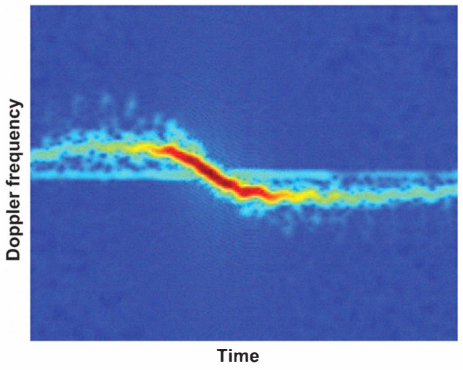

(a) NAM

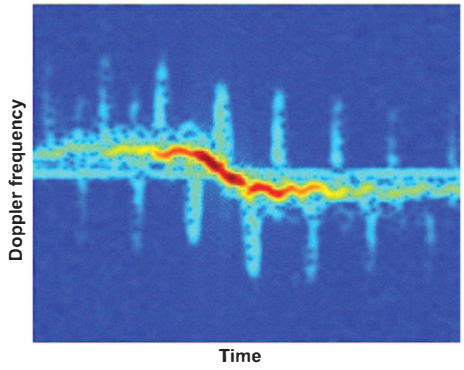

(b) PAM

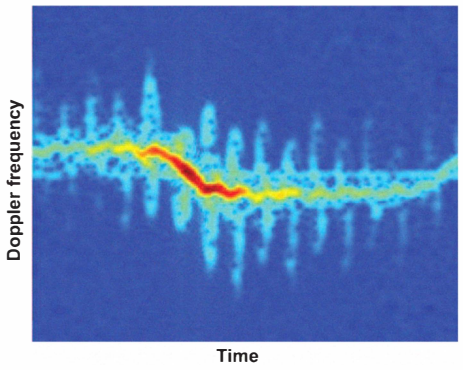

(c) FAM

Fig. 1. Spectrograms of three human arm motions: (c) no-arm swing, (b) one-arm swing and (c) two-arm swing

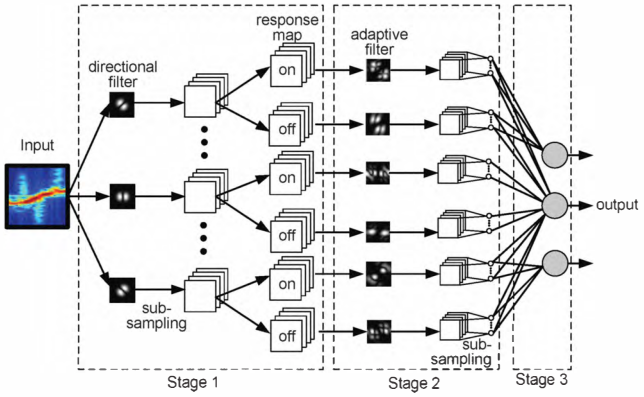

Fig. 2. The Hierarchical image classification architecture.

A. Stage 1 - Oriented Feature Extraction

In the first stage, nonlinear directional filters are used to extract motion energy and directional contrast from the 2-D time-frequency plane. The number of filters, N_1, in the first stage is chosen according to the complexity of the given task; each filter is oriented along an angle $\theta_i = (i-1)\pi/N_1$ ($i = 1, 2, ..., N_1$). The filters are nonrecursive, designed based on feedforward shunting inhibition. The response of the ith filter, oriented along direction θ_i, is given by

$$\mathbf{Z}_{1,i} = \frac{\mathbf{D}_i * \mathbf{I}}{\mathbf{G} * \mathbf{I}}, \tag{1}$$

where $\mathbf{I}$ is the 2-D input pattern, $\mathbf{D}_i$ and $\mathbf{G}$ are 2-D convolution masks, and "$*$" denotes 2-D convolution. We should note that the division operation in Eq. (1) refers to element-by-element matrix division. The convolution mask $\mathbf{D}_i$ is obtained from the first-order derivative of a Gaussian kernel. For a given direction θ_i, the first-order derivative Gaussian kernel is defined as

$$\mathbf{D}_i(x,y) = \cos(\theta_i)\ \mathbf{G}'_x(x,y) + \sin(\theta_i)\ \mathbf{G}'_y(x,y), \tag{2}$$

where

$$\mathbf{G}'_x(x,y) = \partial\mathbf{G}(x,y)/\partial x = \frac{-x}{2\pi\sigma^4}\exp(-\frac{x^2+y^2}{2\sigma^2}), \tag{3}$$

and

$$\mathbf{G}'_y(x,y) = \partial\mathbf{G}(x,y)/\partial y = \frac{-y}{2\pi\sigma^4}\exp(-\frac{x^2+y^2}{2\sigma^2}). \tag{4}$$

The second convolution mask, $\mathbf{G}$, is simply defined as an isotropic Gaussian filter, given by

$$\mathbf{G}(x,y) = \frac{1}{2\pi\sigma^2}\exp(-\frac{x^2+y^2}{2\sigma^2}). \tag{5}$$

Based on preliminary experiments, six directional filters have been selected, which are oriented at angles $\{0, \frac{\pi}{6}, \frac{\pi}{3}, \frac{\pi}{2}, \frac{2\pi}{3}, \frac{5\pi}{6}\}$. The outputs of the six directional filters applied to the Doppler spectrogram of one arm motion are presented in Fig. 3. The figure shows how the different filters emphasize the details of the spectrogram in different directions. This is clearly highlighted by the responses of the $0°$ and $90°$ filters: the filter at zero radian differentiates along the horizontal direction, thereby emphasizing the vertical features, whereas the $\frac{\pi}{2}$ filter differentiates along the vertical direction, which emphasizes horizontal features.

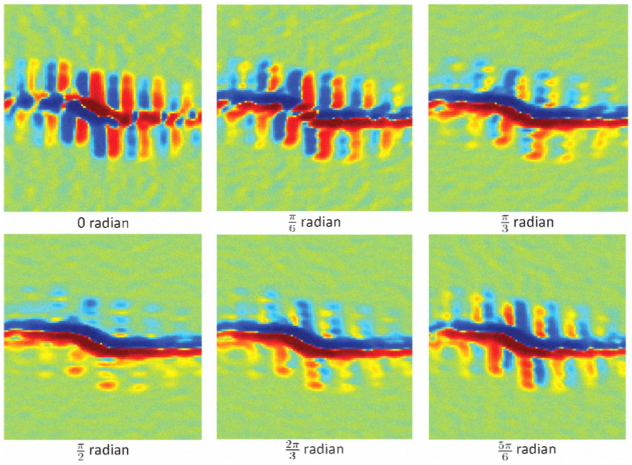

Fig. 3. Outputs produced at Stage 1 from different directional nonlinear filters based on one-arm spectrogram.

In addition to motion energy extraction, the proposed classification model is designed to be robust to small translations and geometric distortions in the input image. This is achieved by reducing the spatial resolution of the filter outputs through down-sampling. The sub-sampling operation employed in the first stage, illustrated in Fig. 4a, decomposes each filter output $\mathbf{Z}_{1,i}$ into four smaller maps:

$$\mathbf{Z}_{1,i} \rightarrow \mathbf{Z}_{1,i,\{1,2,3,4\}}. \tag{6}$$

The first down-sampled map $\mathbf{Z}_{1,i,1}$ is formed from the odd rows and odd columns in $\mathbf{Z}_{1,i}$; the second map $\mathbf{Z}_{1,i,2}$ is formed from the odd rows and even columns, and so on. The rationale of this down-sampling process is to lower the spatial resolution of the filter output without discarding too much information.

Furthermore, inspired by the center-surround receptive fields and the On-Off processing which takes place in the early stages of the mammalian visual systems, each sub-sampled map is divided into an On-response map and an Off-response map by simply thresholding its response:

$$\mathbf{Z}_{1,i,k} \rightarrow \begin{cases} \text{On map}: \mathbf{Z}_{2,2i-1,k} = \max(\mathbf{Z}_{1,i,k}, 0) \\ \text{Off map}: \mathbf{Z}_{2,2i,k} = -\min(\mathbf{Z}_{1,i,k}, 0) \end{cases} \tag{7}$$

Basically, for the on-response map, all negative entries are set to 0, whereas for the off-response map, positive entries are set to 0 and the entire map is then negated. At the end of Stage 1, the features in each sub-sampled map are contrast-normalized, using the following transformation

$$\mathbf{Z}_{3,j,k} = \frac{\mathbf{Z}_{2,j,k}}{\mathbf{Z}_{2,j,k} + \mu}. \tag{8}$$

where μ is the mean value of the absolute response of the output map of the directional filter.

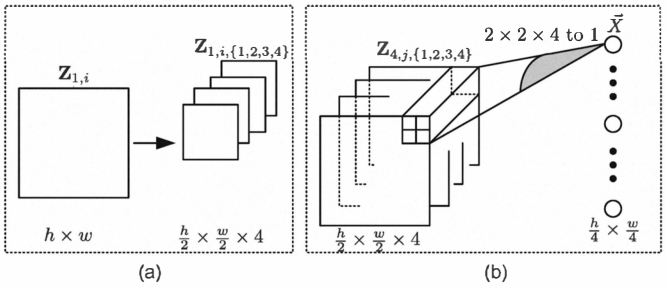

Fig. 4. The sub-sampling operations of Stage 1 (a) and Stage 2 (b).

B. Stage 2 - Learning Intrinsic Motion Features

In stage 2 a set of adaptive filters is used to learn the characteristic features of human motion that can easily be classified into various human motion types. Therefore, the output maps from each directional filter in Stage 1 are processed by exactly two filters in Stage 2: one filter for on-response maps and one for the off-response maps. This implies that the second stage has double the number of filters in Stage 1: $N_2 = 2N_1$. Let $\mathbf{Z}_{3,j,k}$ be the kth sub-sampled input map to the jth filter of Stage 2. The response of stage 2 filter is given by

$$\mathbf{Z}_{4,j,k} = \frac{g\Big(\mathbf{P}_j * \mathbf{Z}_{3,j,k} + b_j\Big) + c_j}{a_j + f\Big(\mathbf{Q}_j * \mathbf{Z}_{3,j,k} + d_j\Big)}, \tag{9}$$

where $\mathbf{P}_j$ and $\mathbf{Q}_j$ are 2-D convolution masks, a_j, b_j, c_j and d_j are bias terms, and f and g are activation functions. All filter parameters in the second stage are adaptable; their desired values are determined using a learning algorithm. The activation functions and biases are added to facilitate convergence of the learning algorithm. During the training phase, a constraint is imposed on the bias term in the denominator of (9) so as to avoid division by zero:

$$a_j \geq \varepsilon - \inf(f), \tag{10}$$

where $\inf(f)$ denotes the lower bound of activation function f, and ε is a small positive constant. Similarly to Stage 1, a sub-sampling operation is performed on the four output maps of each adaptive filter. The four output maps are compressed and arranged into a vector form by averaging each non-overlapping block of size $(2 \times 2 \text{ pixels}) \times (4 \text{ maps})$ into a single output signal. This process is repeated for all output maps produced by the adaptive filters to generate a single column feature vector, as shown in Fig. 4b:

$$\{\mathbf{Z}_{4,j,1}, \mathbf{Z}_{4,j,2}, \mathbf{Z}_{4,j,3}, \mathbf{Z}_{4,j,4}\} \rightarrow \vec{X}, \quad j = 1, 2, \cdots, N_2 \tag{11}$$

Figure 5 shows the response maps of the adaptive filters of stage 2, after training, to one-arm swing motion. The figure illustrates clearly how the micro-Doppler features of the spectrogram are further underlined in Stage 2. These feature are used as inputs to the classification stage to determine the type of motion.

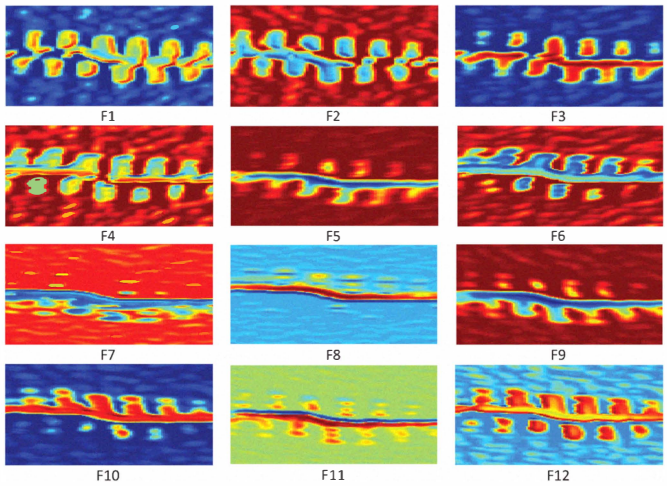

Fig. 5. Outputs produced at Stage 2 from different adaptive filters based on one-arm spectrogram.

C. Stage 3 - Classification

The feature vector extracted by Stage 2 is sent to a classifier, which may be any generic classifier. However, in this paper, a simple linear classifier is used to demonstrate the effectiveness of the HICA in learning the intrinsic motion characteristics. Each class is represented by a linear element, which implements a hyperplane in the feature space. Therefore, the response of the nth output element, denoted by y_n, is given by

$$y_n = \sum_{m=1}^{N_3} w_{nm} x_m + b_n, \tag{12}$$

where w_{nm}'s are adjustable weights, b_n is an adjustable bias term, x_m is the mth element of the input feature vector $\vec{X}$, and N_3 is the number of features. The output class label C_p, corresponding to the pth input pattern, is determined as

$$C_p = \arg\max_n \{y_n\}, \quad n = 1, 2, 3.$$

D. Training Method

Given a training set of P input patterns $\mathbf{I}_1, \mathbf{I}_2, ..., \mathbf{I}_P$ and P corresponding desired outputs $\mathbf{d} = \vec{d}_1, \vec{d}_2, ..., \vec{d}_P$, where $\vec{d}_p$ is the desired output vector associated with the pth input pattern. The adaptation of the parameters of the adaptive filters and the classifier can be formulated as an optimization problem, which minimizes the error between the actual responses of the classifier and the desired outputs. Although other error functions could be used, for simplicity the error function chosen herein is the mean square error (MSE):

$$E_{mse} = \frac{1}{N_4 P} \sum_{p=1}^{P} \sum_{n=1}^{N_4} \Big(d_n^p - y_n^p\Big)^2, \tag{13}$$

where $d_{p,n}$ and $y_{p,n}$ are the nth element of the desired output vector $\vec{d}_p$ and the actual response $\vec{y}_p$, respectively, and N_4 is the dimension of the output vector. The Levenberg-Marquardt

(LM) algorithm [21] is used to learn the optimum adaptive filter parameters in Stage 2 and the parameters of the classifier in Stage 3. The LM algorithm is a fast and effective training method; it combines the stability of the gradient descent with the speed of Newton algorithm. Given that all parameters of the adaptive filters and the linear classifier are arranged as a column vector, $\vec{w} = [w_1, w_2, ..., w_N]^T$. The main steps of the LM algorithm are given as follows.

Step 1: Initialize the trainable coefficients of nonlinear filters in Stage 2 and the parameters of the linear classifier in Stage 3 with random values from a uniform distribution in the range $[-1, 1]$.

Step 2: Perform forward computation to find the outputs of each stage in response to the training patterns.

Step 3: Calculate the weight update at iteration t as

$$\Delta\vec{w}(t) = [\mathbf{J}^T(t)\mathbf{J}(t) + \mu(t)\mathbf{\Phi}]^{-1}\ \mathbf{J}^T(t)\ \mathbf{e}(t) \qquad (14)$$

where $\mathbf{J}(t)$ is the Jacobian of the error function $\mathbf{e}(t)$, $\mathbf{\Phi}$ is the identity matrix and $\mu(t)$ is a regularization term to avoid the singularity problem. During training, the regularization parameter is increased or decreased by a factor of ten, depending on the decrease or increase of the MSE, respectively. The Jacobian matrix can be computed from a modified version of the error-backpropagation algorithm, which is explained in [22].

Step 4: Repeat Steps 2 to 3 until the maximum number of training epochs is reached or the error is below a predefined limit.

IV. Experimental Results

Real data collected from five subjects (A, B, C, D, and E) walking with three different arm motions is divided into two disjoint subsets: a training set and a test set. The training set comprises motion signals from subjects A and B, and the test set includes signals from the remaining three subjects (C, D and E). Furthermore, the training set is sub-sampled by a factor of two and only the odd samples are used for training.

A set of preliminary experiments was performed to determine the optimum configuration of the HICA. The input window is centered around the estimated position of the torso and has size 56×56. In stage 1, there are six directional filters with 9×9 convolution masks, $\mathbf{D}$ and $\mathbf{G}$. The adaptive filters in Stage 2 have 5×5 convolution masks. The linear classifier in Stage 3 has three output nodes representing the three different arm swings: NAM, PAM and FAM. Before extracting overlapping windows as training and test samples, the spectrogram is normalized by setting the maximum peak to one.

In the first experiment, features extracted at different stages are classified with a linear classifier. The classification performance is calculated as a ratio of the number of correctly classified windows over the total number of windows collected from the spectrograms of all three test subjects for different motions. Table I lists the classification rates using features extracted from the raw spectrogram (input windows), Stage 1, and Stage 2 of the HICA. These results show that it is much easier to classify features extracted by the HICA than the raw spectrogram features. Based on the "raw" spectrogram features, a linear classifier can merely achieve 48.7% on the test set. However, using the features extracted by the nonlinear filters in the first stage, the classification rate is improved to 72.2%. Further processing by the adaptive filter in Stage 2 yields a 97.6% classification rate. These results indicate that the classification method can be applied to a spectrogram of a human motion to extract the gait signatures. For further analysis, a confusion matrix is generated and listed in Table II. The main diagonal of the matrix lists the correct classification rate for each human motion. The off-diagonal entries indicate misclassification rates. For example, entry $(1, 3)$ indicates that the proposed method misclassifies 0.98% of the no-arm test data as two-arms motion. Entries in the second and third rows show that the classifier also has some difficulty in distinguishing between one-arm and two-arms motions.

TABLE I
CLASSIFICATION PERFORMANCES AT DIFFERENT STAGES OF THE PROPOSED METHOD.

	classification rate (%)	
	Training set	Test set
Features extracted from spectrogram	100	48.69
Features extracted from Stage 1	100	72.22
Features extracted from Stage 2	100	97.65

TABLE II
CONFUSION MATRIX LISTING THE CLASSIFICATION RATES OF THREE HUMAN MOTIONS.

	Labeled No arms	Labeled One arm	Labeled Two arms
No arms	99%	0%	0.98%
One arm	0.78%	97.5%	1.76%
Two arms	0%	3.53%	96.5%

However, the results presented in Table II are based on classification of short overlapping time-windows of length 4.7s. By contrast, many existing methods use the entire frame to classify the motion of the subject. For the proposed method, only a short segment, comprising several windows, is sufficient to achieve perfect classification. In order to classify a segment of the spectrogram, a series of overlapping windows are extracted and processed by the proposed method to produce a set of classification scores, which are then aggregated using the majority voting rule. In the second experiment, each spectrogram frame is divided into 4 non-overlapping segments. From each segment, a number of overlapping input windows are classified by the proposed method. Figure 6 shows the classification performance as a function of the number of segments per frame. Dividing the spectrogram into 3 segments, and classifying each segments individually, the proposed classification method achieves perfect results. However, when dividing each frame into 4 segments, one of the segments for the no-arms motion was misclassified; hence, there is a decrease in the average classification rate. In [11], Principal

component analysis (PCA) was combined with a minimum distance classifier using the Mahalanobis distance to classify the spectrogram of human motion. For no-arms, one-arm and two-arms motions, the best classification rates achieved, based on the entire spectrogram frame, were 82.5%, 69.1% and 70.7%, respectively. In comparison, the proposed method achieves perfect classification of shorter time segments using the same test data. One possible reason why PCA achieves low classification rates is that by projecting the data onto a subspace of lower dimension, the periodicity of the arm swings is not retained. On the other hand, the proposed classification method captures this vital information by processing a 2D input of joint time-frequency representation.

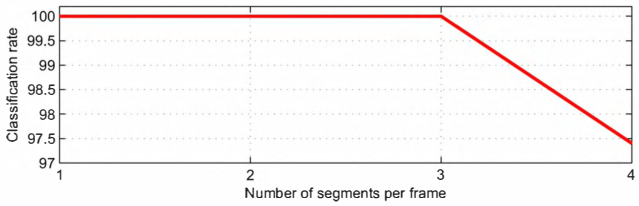

Fig. 6. Average classification rate of the three human motions as a function of the numbers of classified segments per frame.

V. Conclusion

A three-step classifier employing both fixed directional and adaptive filters, in addition to a linear classifier, is introduced for classifying three types of human walking. The filters are applied in the time-frequency domain which depicts the Doppler signal power distribution over time and frequency. Three types of arm motion are considered; free arm swings, one-arm confined swings, and two-arm confined swings. The proposed classifier determines the optimum time-frequency window for training and testing, and is able to underscore and extract the distinct Doppler features underlying the three motions. The data used for testing and training correspond to five subjects moving towards and away from the radar with zero aspect angle, and with non-obstructed line of sight. The paper shows the importance of each step of the classifier in improving the classification rates. The attractiveness of the proposed classifier lies in its robustness to data misalignments, forward/backward walking motions, including the acceleration-deceleration phases exhibited when turning, and to the specific quadratic distribution used for time-frequency signal representations.

Acknowledgment

This work is supported in part by a grant from the Australian Research Council (ARC).

References

[1] M. Amin and K. Sarabandi (Guest Editors), "Special issue on remote sensing of building interior," *IEEE Transactions on Geoscience and Remote Sensing*, vol. 45, no. 5, pp. 1267–1268, 2009.

[2] M. Amin (Guest Editor), "Special issue on advances in indoor radar imaging," *Journal of the Franklin Institute*, vol. 345, no. 6, pp. 556–722, 2008.

[3] D. G. Falconer, K. N. Steadman, and D. G. Watters, "Through-the-wall differential radar," in *Proc. SPIE Conf. on Command, Control, Communications, and Intelligence Systems for Law Enforcement*, vol. 2938, 1996, pp. 147–151.

[4] S. Borek, "An overview of through the wall surveillance for homeland security," in *Proc. of the 34th Workshop on Applied Imagery and Pattern Recognition*, 2005, p. 6.

[5] A. Hunt, "Image formation through walls using a distributed radar sensor array," *Proc. of the 32nd Applied Imagery Pattern Recognition Workshop*, pp. 232–237, 2003.

[6] L. Cohen, *Time-frequency analysis*. Prentice Hall, 1995.

[7] P. V. Dorp and F. C. A. Groen, "Human walking estimation with radar," *IEE Proc. Radar, Sonar and Navigation*, vol. 150, no. 5, pp. 356– 365, 2003.

[8] V. C. Chen, "Analysis of radar micro-doppler signature with time-frequency transform," in *Proc. of the IEEE Workshop on Statistical Signal and Array Processing (SSAP)*, Pocono, PA, 2000, pp. 463–466.

[9] G. E. Smith, K. Woodbridge, and C. J. Baker, "Multistatic micro-doppler signature of personnel," *IEEE Radar Conference*, pp. 1–6, 2008.

[10] Y. Kim and H. Ling, "Human activity classification based on microdoppler signatures using a support vector machine," *IEEE Transactions on GeoScience and Remote Sensing*, vol. 47, no. 5, pp. 1328–1337, 2009.

[11] B. G. Mobasseri and M. Amin, "A time-frequency classifier for human gait recognition," in *SPIE Defense, Security and Sensing*, vol. 7306, 2009.

[12] B. Lyonnet, C. Ioana, and M. Amin, "Human gait classification using microdoppler time-frequency signal representations," *Proc. of IEEE International Radar Conference* (RADAR 2010), Washington D.C., 10-14 May 2010.

[13] F. H. C. Tivive, A. Bouzerdoum, S. L. Phung, and K. M. Iftekharuddin, "Adaptive hierarchical architecture for visual recognition," *Applied Optics*, vol. 49, no. 10, pp. B1–B8, 2010.

[14] S. J. Mitchell and R. A. Silver, "Shunting inhibition modulates neuronal gain during synaptic excitation," *Neuron*, vol. 38, no. 3, pp. 433–445, 2003.

[15] S. A. Prescott and Y. D. Koninck, "Gain control of firing rate by shunting inhibition: Roles of synaptic noise and dendritic saturation," *Proceedings of the National Academy of Sciences of the United States of America*, vol. 100, no. 4, pp. 2076-2081, 2003.

[16] G. Arulampalam and A. Bouzerdoum, "A generalized feedforward neural network architecture for classification and regression," *Neural Networks*, vol. 16, no. 5-6, pp. 561–568, 2003.

[17] G. Arulampalam and A. Bouzerdoumn, "Training shunting inhibitory artificial neural networks as classifiers," *Neural Network World*, vol. 10, no. 3, pp. 333–350, 2000.

[18] A. Bouzerdoum, "Classification and function approximation using feed-forward shunting inhibitory artificial neural networks," in *Proc. of the IEEE-INNS-ENNS International Joint Conference on Neural Networks*, vol. 6, 2000, pp. 613–618.

[19] H. N. Cheung, A. Bouzerdoum, and W. Newland, "Properties of shunting inhibitory cellular neural networks for colour image enhancements," in *Proc. of the Sixth International Conference on Neural Information Processing*, vol. 3, 1999, pp. 1219–1223.

[20] T. Hammadou and A. Bouzerdoum, "Novel image enhancement technique using shunting inhibitory cellular neural networks," *IEEE Transactions on Consumer Electronics*, vol. 47, no. 4, pp. 934–940, 2001.

[21] M. T. Hagan and M. Menhaj, "Training feedforward networks with the marquardt algorithm," *IEEE Transactions on Neural Networks*, vol. 5, pp. 989–993, 1994.

[22] F. H. C. Tivive and A. Bouzerdoum, "Efficient training algorithms for a class of shunting inhibitory convolutional neural networks," *IEEE Transactions on Neural Networks*, vol. 16, no. 3, pp. 541– 556, 2005.